Nuclear Materials and Energy 28 (2021) 101037

Contents lists available at ScienceDirect

Nuclear Materials and Energy

journal homepage: www.elsevier.com/locate/nme

An examination of the Neutral Penetration Model $1/n_{e,ped}$ scaling for its validity of spatially varying neutral sources

J. Simpson [a,b,*], D. Moulton [a], C. Giroud [a], F. Casson [a], M. Groth [b], A. Chankin [c], L. Horvath [a], D. S. Gahle [d], L. Garzotti [a], G. Corrigan [a], F. Kochl [a], JET contributors[1]

[a] CCFE, Culham Science Centre, Abingdon OX14 3DB, UK
[b] Aalto University, FI-00076 AALTO, Espoo, Finland
[c] Max-Planck-Institut für Plasmaphysik, Boltzmannstraße 2, D-85748 Garching, Germany
[d] University of Strathclyde, 16 Richmond St, Glasgow G1 1XQ, UK

ARTICLE INFO

Keywords:
Density pedestal prediction
Neutral penetration
Neutral penetration model
1/neped scaling

ABSTRACT

The core transport code, JETTO, coupled to the neutral Monte Carlo code, EIRENE, has been used to examine the sensitivity of the JET H-mode pedestal to the neutral flux crossing the separatrix. The Neutral Penetration Model (NPM) [Groebner et. al., Physics of Plasmas 9, 2134 (2002)] predicts the width of the density pedestal along the neutral path to scale with the inverse of its height: $1/n_{e,ped}$. By keeping the same physics assumptions in the NPM, and setting the deuterium atoms to cross the separatrix at the same location as the synthetic diagnostic line of sight (i.e. at the outer mid-plane, OMP), we were able to reproduce this scaling in JETTO-EIRENE. However, when the atoms were set to cross the separatrix at the X-point (more consistent with EDGE2D-EIRENE simulations of JET H-modes), the density width at the OMP was found to be much more sensitive to the pedestal height (approximately proportional to $1/n^2_{e,ped}$). This is attributed to a radial variation in the poloidal flux expansion from OMP to X-point, over the range of ionisation mean free path lengths explored in the scan. Accounting for this variation allowed the expected scaling at the OMP to be recovered. Implications are discussed for experimental comparisons to the NPM and its application to pedestal prediction models.

1. Introduction

An H-mode plasma [1] has a distinct characteristic of a steep gradient region at the edge of the plasma known as the pedestal. This steep gradient region is present in the temperature and density and can be quantified by its height and width. Typically an increase in the pressure pedestal height leads to an increase in the core pressure, due to stiff profile [2] which leads to increased fusion yield [3]. Thus, predicting the pedestal height and width is key for predicting the confinement of future machines and experiments.

Models such as EPED1 [4,5] attempt to predict the pressure pedestal height and width. Calculating the ideal magneto–hydrodynamics (MHD) stability of the pressure pedestal and a model for the pressure pedestal width (pressure pedestal width is proportional to pedestal β poloidal) EPED can predict the pressure pedestal width and height self consistently. However, the predictive capability of EPED is limited by: the pedestal density height ($n_{e,ped}$,) as input and, assuming the density pedestal width (Δ_{ne},) is equal to the temperature and pressure pedestal widths. It is therefore desirable to have a model which can predict $n_{e,ped}$, and Δ_{ne}, which would allow models such as EPED to not make assumptions about the density profile.

The density profile is not always known *a priori* and hence neither is density pedestal height, ($n_{e,ped}$,) or width (Δ_{ne},). It is clear from experiments that the density pedestal is dependent on many operational parameters such as divertor configuration, plasma current and triangularity [6] [7] [8] [9]. The only analytic model (at least known to these authors) to predict the density pedestal is the neutral penetration model (NPM) [10]. A key prediction of the NPM is that the density pedestal height ($n_{e,ped}$,) is inversely related to the density pedestal width (Δ_{ne},).

A similar model to EPED, EUROPED uses the NPM as a model for density pedestal prediction (using the $1/n_{e,ped}$, scaling) [11]. Predictions

* Corresponding author.
E-mail address: james.simspon@ukaea.uk (J. Simpson).
[1] See the author list of E. Joffrin et al. accepted for publication in Nuclear Fusion Special issue 2019, https://doi.org/10.1088/1741-4326/ab2276.

https://doi.org/10.1016/j.nme.2021.101037
Received 31 July 2020; Received in revised form 20 June 2021; Accepted 23 June 2021
Available online 6 July 2021

by the EUROPED model are sensitive to the poloidal position of the neutral source, which is accounted for in the NPM by the E function. The E function is a measure of the radial poloidal flux expansion between the poloidal position of where the neutrals enter the plasma, and the poloidal position of the measurement of the density profile, typically the outer midplane (OMP) on JET. Modelling using scrape off layer transport codes (e.g. EDGE2D-EIRENE) investigated the poloidal distribution of neutrals crossing the separatrix finding that dominant neutral flux originated from the divertor and was localised the around the X-point [12,13].

Experimental observations however are not always consistent with the predictions of the NPM specifically that $n_{e,ped}$, is related to the inverse of Δ_{ne}, [14,15]. Importantly for the machine considered in this paper, JET, the $1/n_{e,ped}$, scaling is only observed at a low gas rate [6].

In this work, we compare simulations to the NPM $1/n_{e,ped}$, prediction of the pedestal density width. We examine what happens to this scaling when particular assumptions of the NPM are relaxed. Further, we examine closely the E function and whether the assumption it is a scalar constant is reasonable and the implication if it is not.

2. The neutral penetration model

In this section, we reproduce the important details of the neutral penetration model [10], and highlight the role played by poloidal flux expansion between the location where deuterium atoms cross the separatrix and the location where the density profile is measured.

Consider the electron and atomic density along the path of a mono-energetic beam of deuterium atoms crossing locally into the core at a single poloidal location on the separatrix. The continuity equations for electrons and neutrals are:

$$D_{\perp}\frac{d^2 n_e}{dx^2} = n_n(x) n_e(x) < \sigma v_e >_{iz} \tag{1}$$

$$v_0 \frac{dn_n}{dx} = -n_n(x) n_e(x) < \sigma v_e >_{iz} \tag{2}$$

where x is the negative of the distance (towards the core of the plasma) from the separatrix ($x = 0$) along the neutral beam, $D_{\perp}$ is the particle diffusion coefficient (assumed constant), $< \sigma v_e >_{iz}$ is the ionisation rate, n_n is the neutral density (here we mean deuterium atoms whenever referring to neutrals), n_e is the electron density and v_0 is the velocity of the neutral beam originating at the separatrix. Following reference [10], Eqs. 1 and 2 have the solution:

$$n_e(x) = n_{e,ped}\ \tanh\left(\tanh^{-1}\left[\frac{n_{e,sep}}{n_{e,ped}}\right] - \frac{< \sigma v_e >_{iz}}{2v_0} n_{e,ped} x\right), \tag{3}$$

where $n_e(x = 0) = n_{e,sep}$ is the separatrix electron density and $n_e(x \to -\infty) = n_{e,ped}$ is the pedestal density height.

Neutrals are unlikely to cross the separatrix at the same location where the electron density profile is measured. As a result, before the NPM can predict the profile along the diagnostic line of sight, the distance along the neutral path x must be mapped (assuming n_e to be a flux function) to the distance along the diagnostic line of sight x_m (as for x, x_m is defined to be positive away from the magnetic axis and zero at the separatrix). The 'poloidal flux expansion function'

$$E = \frac{dx/d\psi}{dx_m/d\psi}, \tag{4}$$

which measures the change in poloidal flux ψ along the neutral path relative to the change in ψ along the diagnostic line of sight, provides this mapping. It is worth noting that to transform between neutral path, x to the diagnostic line of sight x_m the following can be applied:

$$x = x_m \cdot E \tag{5}$$

Along the diagnostic line of sight, x_m, the NPM therefore predicts the density profile:

$$n_e(x_m) = n_{e,ped} \tanh\left(tanh^{-1}\left[\frac{n_{e,sep}}{n_{e,ped}}\right] - \frac{< \sigma v_e >_{iz}}{2v_0} n_{e,ped} E x_m\right), \tag{6}$$

From Eq. (6), the characteristic distance to achieve $n_{e,ped}$, is given as:

$$\Delta_{ne,m} = \frac{\Delta_{ne}}{E} = \frac{2v_0}{E < \sigma v_e >_{iz} n_{e,ped}} \tag{7}$$

Here, $\Delta_{ne,m}$ is the pedestal electron density width along the diagnostic line of sight and Δ_{ne} is the width along the neutral path. Assuming everything but $n_{e,ped}$, is constant in Eq. (7), yields the key prediction from the NPM that $\Delta_{ne} \propto 1/n_{e,ped}$. In Section 4 we consider the case where $< \sigma v_e >_{iz}$ is not constant and that v_0 can vary due to charge exchange. Note where E varies over the range of $\Delta_{ne,m}$ explored in a scan, the scaling ($\Delta_{ne} \propto 1/n_{e,ped}$) predicted by Eq. (6), can no longer be expected to hold.

The last point above is a key focus of this paper. Consider, for example, the poloidal flux expansion function for the JET equilibrium used throughout this paper (details in Section 3). Fig. 1b shows E as a function of $x_m = R_{OMP} - R_{sep}$, for the case where the neutral path is vertically upward at the X-point and the diagnostic line of sight is along the OMP (black and red lines in Fig. 1a, respectively). The values of $\Delta_{ne,m}$ calculated from fits to the simulations presented in this paper range from 0.015 m to 0.165 m. At the lower end of this range, neutrals crossing at the X-point in the narrowest width (highest density) simulations ionise in a region near the separatrix, where E is high. In contrast, at the upper end of the range, neutrals crossing the X-point in the largest width (lowest density) simulations ionise further away from the separatrix, where E is lower. As a result, E in Eq. (7) is effectively an increasing function of $n_{e,ped}$, so that the NPM predicts Δ_{ne}, to be more sensitive to $n_{e,ped}$, along the OMP than the $1/n_{e,ped}$, scaling predicted along the neutral path. Noting that typically, the experimental JET density pedestal width is approximately in the range of 1–4 cm [16], which is a similar range which E varies over (Fig. 1b).

As an important aside before proceeding, we note that the standard method for calculating the density pedestal width and height in experiments is to use a "modified tanh" (mtanh) function [17], which allows for a non-zero gradient in the core. Typically on JET, this modified tanh is applied with a constant density offset to avoid negative values in the SOL. Assuming no core gradient, and an appropriate density offset, the standard mtanh function collapses to a function of the same form as Eq. (6):

$$n_e(x_m) = n_{e,ped} \tanh(a - x/b), \tag{8}$$

where a and b are fitting constants. This is important because in Section 4 we will fit density profiles to Eq. (6) (with fixed E). This is the same procedure as typically done in experiments, but assuming zero core gradient and an appropriate density offset[2].

3. JETTO-EIRENE simulation set up

A recent JET H-mode discharge (shot number 92168 with $I_p = 1.36\ MA$ and $B_t = 1.9\ T$ at 44.62 s), operated in a vertical (inner) and horizontal (outer) target configuration, was chosen for this study. This shot was chosen because good diagnostic data for both the pedestal and the core was available [18], as was a well constrained interpretative

[2] in Eq. (1) in [17], this would be the same as setting the parameter $a_{sol} = -n_{e,ped}$ and $a_{slope} = 0$. Note that although setting a_{sol} negative implies negative densities beyond the separatrix, Eq. (6) is not meant to be applied in that region anyway. In Section 4 the conclusions drawn are the same irrespective of whether we fit to Eq. (6) or Eq. (1) in [17] with $a_{sol} = 0$, as is more typical in JET analysis

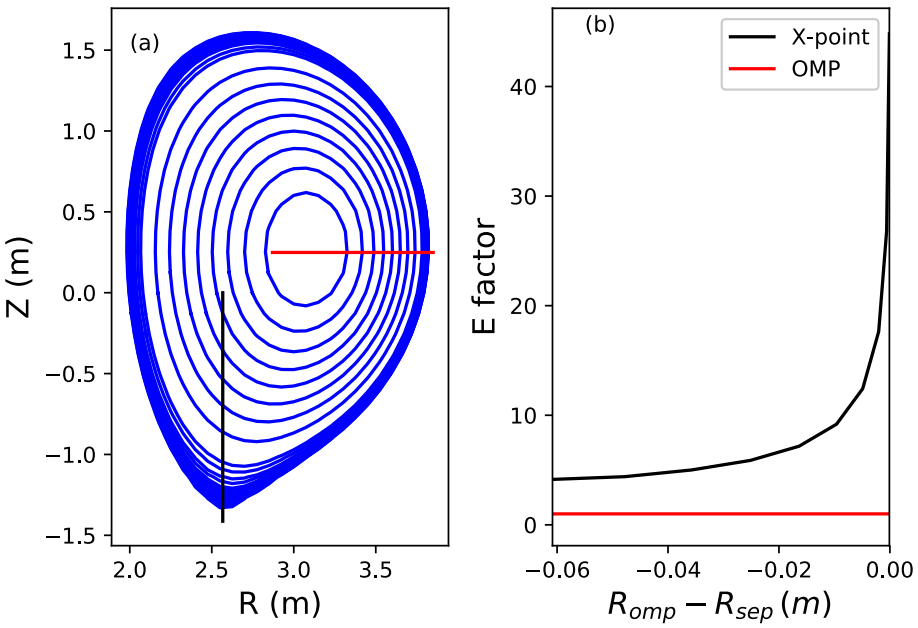

Fig. 1. (a) Equilibrium used for the JETTO-EIRENE simulations denoting the injection location of the point source of neutrals (on the separatrix) at the outer midplane (red) and X-point (black). The extent of the line demonstrates the direction of the initial velocity vector of the neutrals. (b) Poloidal flux expansion factor E (defined in Section 2, Eq. (4)) as a function of radial distance at the outer midplane. The black line is the E function calculated at the X-point and the red line is E function calcul.ated at the OMP.

EDGE2D-EIRENE [19] [20] simulation [18]. The 1D transport code JETTO [21], coupled to the 3D neutral code EIRENE [20], was run with non-evolving background profiles for the electron temperature T_e and for the ion temperature T_i and separatrix electron density $n_{e,sep} = 1.68 \times 10^{19}\ m^{-3}$. Two scenarios were compared: (i) spatially constant T_e and T_i profiles fixed at 800 eV (so that $<\sigma v_e>_{iz}$=constant), and no charge exchange (in this case a match to the NPM was expected); (ii) spatially varying T_e and T_i profiles, fixed to the experimentally measured profiles from Thomson scattering (for T_e) and edge charge exchange diagnostics (for T_i). In this latter case the JETTO separatrix temperature boundary conditions were taken from the matched EDGE2D-EIRENE simulation, as follows: $T_{e,sep} = 116\ eV, T_{i,sep} = 480\ eV$ [3] as was the aforementioned $n_{e,sep}$. The magnetic equilibrium was also kept fixed, according to the EFIT reconstruction at 44.62 s. The electron density equation was evolved, assuming a fixed perpendicular diffusivity (for consistency with the NPM) of $D_\perp = 0.05\ m^2 s^1$. This value was the same as used in the pedestal region of the experimentally matched EDGE2D-EIRENE simulation. In all simulations, for consistency with the NPM assumptions (where v_0 is constant), a beam of fixed-energy neutrals were injected from the separatrix into the simulations, at a single poloidal location. This beam had an energy of 156 eV, taken from the EDGE2D-EIRENE simulation. Note that JETTO is a 1D code, while EIRENE is 3D. When EIRENE simulates neutral trajectories, the 1D OMP profile from JETTO is filled out onto a 3D grid, assuming all quantities to be poloidally and toroidally constant. In the other direction, from EIRENE to JETTO, the EIRENE-calculated ionisation profiles are poloidally averaged before being passed to JETTO. The ionisation rates for the deuterium atoms came from the HYDHEL database (Eq. H.2 2.1.5, in reference [22]), and depend only on T_e (the coronal approximation). For all simulations, the neutral recombination process in EIRENE is turned off.

To obtain density scans in the simulations, we varied the neutral flux crossing the separatrix. The sensitivity of the neutral influx location was assessed by injecting neutrals into the simulations either at the OMP or at the X-point, along the trajectories marked in Fig. 1a. The matched EDGE2D-EIRENE simulation suggests that neutrals do indeed enter around the X-point in shot 92168. Fig. 2 shows the neutral flux density crossing the separatrix in that simulation, as a function of the poloidal

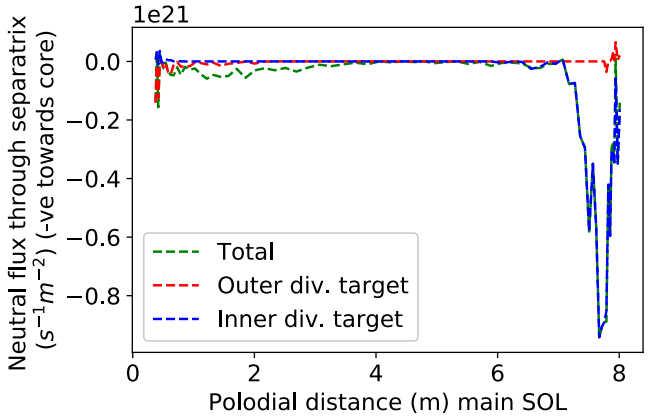

Fig. 2. Neutral source at individual poloidal locations along the separatrix from a EDGE2D-EIRENE simulation. Each line shows the neutral flux density crossing the separatrix which originate from a particular neutral source. Blue line - inner divertor target, red line - outer divertor target and the green line is the sum off all neutral sources. Note that negative direction is towards the core. The extremes of the x axis are located in real space adjacent to each other.

distance along the separatrix (increasing from zero at the outer target). Negative values here mean that neutrals are crossing into the core. The total neutral flux density (green) is broken down according to the origin of the neutrals. We see that most of the neutrals crossing into the core do so around the inboard side of the X-point, and originate from inner target recycling (blue). This flux through the X-point is consistent with previous EDGE2D-EIRENE simulations of L-mode JET discharges [12].

The JETTO-EIRENE simulation setup described above is clearly a strong simplification of the JET pedestal. Our goal here is not to reproduce experiment, but rather to create a sufficiently simplified simulation so that the profiles predicted by the NPM are indeed reproduced. Such simulations are useful because they allow us to separate discrepancies that arise because the NPM assumptions themselves are wrong, and from discrepancies that arise because of the application of the NPM. In addition, starting from an agreement with the NPM as a reference, it is useful to see how additional physics beyond the NPM, in the simulation effects that agreement (for example by including realistic temperature profiles and charge exchange).

[3] Note that the effect of this unexpectedly high value of $T_{i,sep}$ on the results presented here is negligible

4. Results

4.1. $1/n_{e,ped}$, scaling when neutrals enter at the OMP

Consider first the simulation where we have deliberately met the assumptions of the NPM namely: (i) fixed constant electron diffusivity; (ii) fixed neutral velocity; (iii) $<\sigma v_e>_{iz}$ is constant (achieved by setting a spatially constant T_e profile) and (iv) charge exchange is not considered. The neutrals are injected at the OMP separatrix along the same path as the density profile is measured and a scan in source strength from 7.75×10^{21} to 93×10^{21} atoms per second is conducted. Importantly this set-up results in $E = 1$ because measurement of the density profile and injection of the neutrals are at the same poloidal location. The predicted profiles are fitted using Eq. (6). Specifically the free fitting parameters are pedestal width (Δ_{ne}), the pedestal height ($n_{e,ped}$,) and $\tanh^{-1}(n_{e,ped}/n_{e,sep})$. The fitted density profile for the lowest and highest neutral influx rates are shown in Fig. 3a and Fig. 3c. In this case, a near-perfect agreement is obtained between the simulated density profiles and Eq. (6). The average fraction deviation between the fit and simulated data is in the range of 0.3 −0.4%. We define average fractional deviation (χ) as the mean of R (average residual) where $R = abs((y - f)/y)$ where y is the simulated data and f is the fitted data. The $1/n_{e,ped}$, scaling is observed as shown in Fig. 4a by black dashed line ($\chi = 0.6\%$) which is a fit to Δ_{ne}, and $n_{e,ped}$, denoted by the star markers on Fig. 4a. Note that $2\Delta_{ne}$ is plotted (in Fig. 4a and proceeding figures) as to be directly comparable to a pedestal width predicted by Eq. (1) in reference [17] which is typically used for experiment.

In an additional neutral injection rate scan, the assumption that the ionisation rate is constant (implemented by using the fixed experimental T_e profile) is relaxed and the CX process is turned on in the simulation, using the experimental T_i profile. This is more representative of a real pedestal where T_e can vary significantly over the width of the pedestal. The ionisation rate ($<\sigma v_e>_{iz}$) is now radially varying along x. The same scan in the neutral source strength from 7.75×10^{21} to 93×10^{21} atoms per second is injected at the OMP. Importantly this setup keeps the $E =$

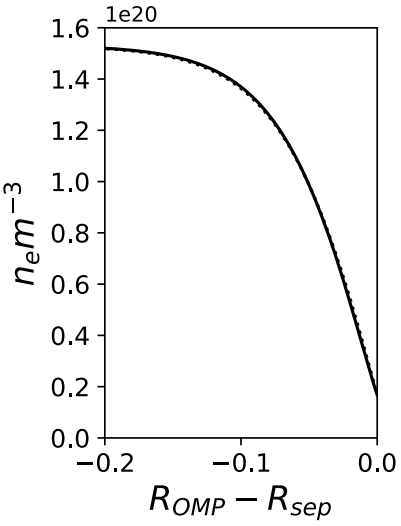

(a) OMP, $\chi = 0.4\%$

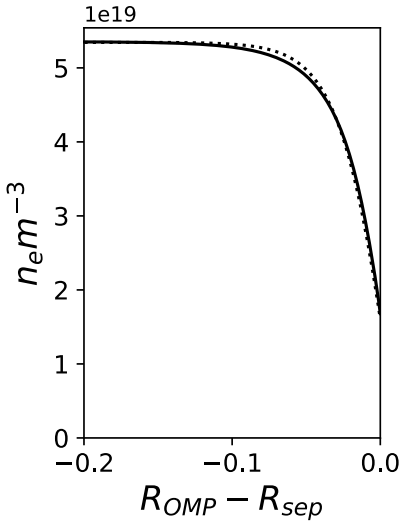

(b) X-point, , $\chi = 0.5\%$

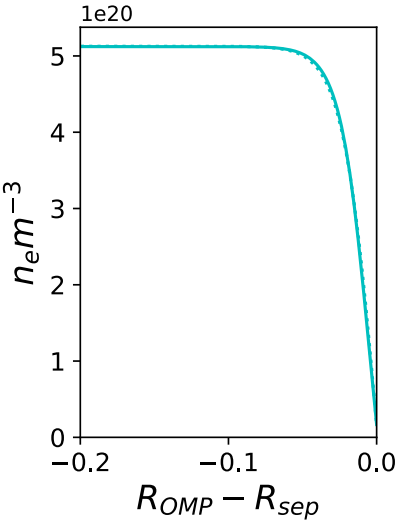

(c) OMP, $\chi = 0.4\%$

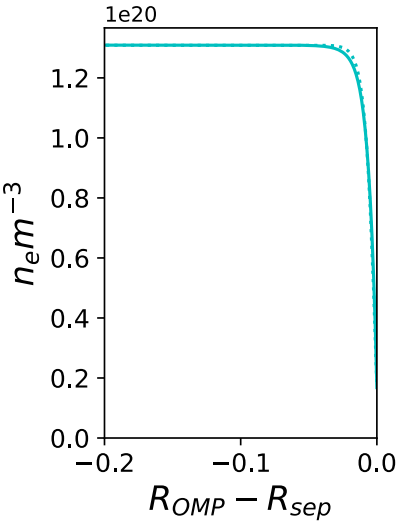

(d) X-point, $\chi = 0.2\%$

Fig. 3. Density profiles (solid lines) predicted by JETTO-EIRENE fitted by Eq. (6) (dotted lines). (a) and (b) have the neutral source placed at the OMP and X-point respectively, with a deuterium neutral source of 7.75×10^{21} atoms per second. (c) and (d) have the neutral source placed at the OMP and X-point respectively, with a deuterium neutral source of 93×10^{21} atoms per second.

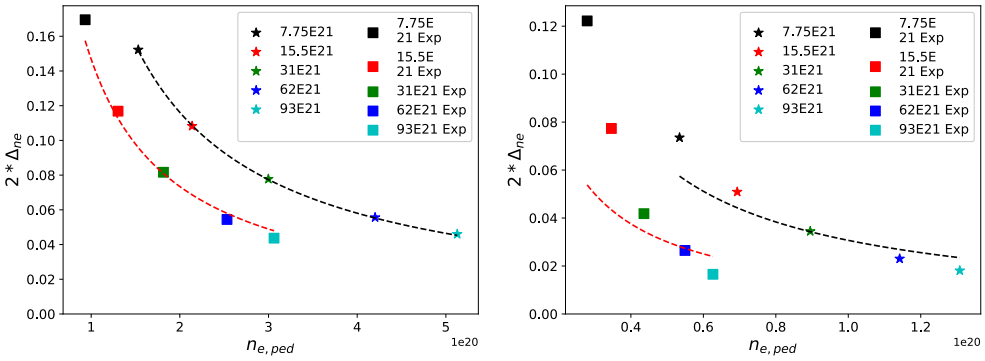

(a) Red dashed line $\chi = 5\%$
Black dashed line $\chi = 0.6\%$

(b) Red dashed line $\chi = 33\%$
Black dashed line $\chi = 16\%$

Fig. 4. A neutral source scan where the neutral source is placed either at the (a) outer midplane or (b) X-point. Δ_{ne}, and $n_{e,ped}$, are calculated from fitting Eq. (6) to the predicted density profiles from JETTO-EIRENE. The x-axis for fit is taken to be the coordinate at the OMP (red line in Fig. 1a). The stars represent a simulation set up with a constant temperature profile and charge exchange (CX) turned off and the squares using the experimental T_e and T_i profiles and CX turned on. The dashed lines are the $1/n_{e,ped}$, fits to Δ_{ne}, and $n_{e,ped}$, of each data set (stars or squares). The neutral source scan shown here ranges from 7.75×10^{21} to 93×10^{21} atoms per second denoted by changing colour as shown on the legen.d of the figure.

1. Interestingly, the $1/n_{e,ped}$, scaling is still observed in this setup (square markers Fig. 4a and red dashed line which shows $1/n_{e,ped}$, fit to the markers with a $\chi = 5\%$), indicating that the assumption of no CX and constant ionisation rate is reasonable. Noting that the fits to Eq. (6) for this data set (denoted by the squares in Fig. 4a) had a χ in the range of 0.3 −1.3%.

4.2. $1/n_{e,ped}$, scaling when neutrals enter at the X-point

Motivated by the EDGE2D-EIRENE simulations presented in Fig. 2 we repeat the same analysis presented in the previous section but placing the neutral source at the X-point rather than the OMP. This is now to investigate the effect of the radially varying E (Fig. 1b). The same neutral source scan over 7.75×10^{21} to 93×10^{21} atoms per second with the source placed at the X-point was conducted. This neutral source scan was conducted firstly with a constant T_e and then the experimental T_e and T_i (and turning on CX process in the simulation).

The density profile of the neutral source scan were observed along the OMP and so x_m is now different to the coordinate x which the neutrals are injected along. Specifically, x is directed along the black line in Fig. 1a and x_m along the red line in Fig. 1a. The consequence of this is that E is now not equal to 1 as in the previous section but is a radial varying function, as shown in Fig. 1b. The E function varies quite significantly (approximately a factor 8, Fig. 1b) over the pedestal widths (0.01 m −0.12 m) predicted by the scan (Fig. 4b). Hence the relation $1/n_{e,ped}$, scaling is not expected. This indeed is what is observed, Fig. 4b (star and square markers) show that the $1/n_{e,ped}$, scaling is not followed, and in fact becomes more akin to $1/n^2_{e,ped}$. Comparing like for like simulation setups, constant T_e and CX off (star markers Figs. 4a & 4b) when injecting neutrals at the OMP χ for $1/n_{e,ped}$, fit increases significantly from 0.6% to 16% when injecting neutrals at the X-point (black dashed line on Figs. 4a & 4b). A large change in χ (5% to 33%) is also seen for simulations assuming experimental T_e, T_i and CX turned on (red dashed line on Figs. 4a & 4b). Comparing the density profile fits (of Eq. 6) of similar neutral source rates (lowest rate - Fig. 3a versus Fig. 3b and highest rate - Fig. 3c versus Fig. 3d) show that when injecting neutrals from the OMP or X-point regardless of neutral source strength χ changes very little (approximately 0.2% change). The assumption of a tanh fit is still appropriate for the predicted density profiles even when the neutral source is placed at the X-point (Figs. 3b & 3d). The fact that the E function varies over the range pedestal widths explored in this scan is the driving factor for why the $1/n_{e,ped}$, scaling is not observed in the simulations where the neutral source is placed at the X-point.

To recover the $1/n_{e,ped}$, scaling when the neutral source is placed at the X-point we need to make $E = 1$ again, i.e. remove the spatial dependence from the E function. To do this, a remapping of the density profiles predicted by JETTO observed at the OMP, to a coordinate along the X-point given by the black line in Fig. 1a is performed. Using the real (Z) coordinates given along the black line in Fig. 1a the intersection of the normalised ψ values with this line are recorded. This can be used to transform the measured density profile at the OMP to the black line in Fig. 1a. The same result could be achieved by using Eq. 5 and multiplying the OMP coordinate by the radially varying E function from Fig. 1b. Eq. (6) can now be fitted to the remapped density profile (to fit for Δ_{ne}, and $n_{e,ped}$,) but using this new (transformed) coordinate along the X-point. χ for these fits now falls into the range of 0.7 −2.6%. The $1/n_{e,ped}$, scaling is now observed shown in Fig. 5 by the square and star markers, where the dashed lines shows the $1/n_{e,ped}$, scaling, which are fitted to the star and square markers respectively. The χ for this $1/n_{e,ped}$, scaling fit has reduced by an order of magnitude (for both data sets denoted by star and square markers) compared to the χ when the fit is carried out on the density profile measured at the OMP (with the neutral source placed at the X-point). Thus showing that indeed this $1/n_{e,ped}$, fit (dashed lines Fig. 5) is significantly better compared to $1/n_{e,ped}$, fit of Δ_{ne}, and $n_{e,ped}$, when measured at the OMP (dashed lines Fig. 4b). Note that now the density pedestal width (Δ_{ne}) and height ($n_{e,ped}$,) is now given at the X-point and not the OMP.

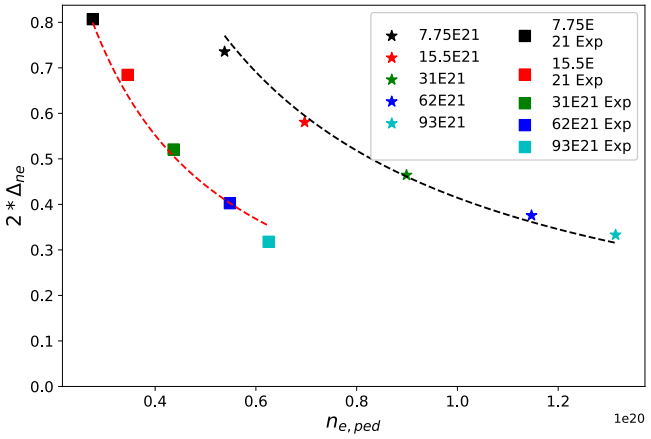

Fig. 5. A neutral source scan where the neutral source is placed at the X-point. Δ_{ne}, and $n_{e,ped}$, are calculated from fitting Eq. (6) to the predicted density profiles from JETTO-EIRENE. The x-axis for the Eq. (6) is taken to be the coordinate at the X-point where the neutral source is injected along (black line in Fig. 1a). The stars represent a simulation set up with a constant temperature profile and charge exchange (CX) turned off and the squares using the experimental T_e and T_i profiles and CX turned on. The black dashed line is the $1/n_{e,ped}$, fit to the star markers with a $\chi = 4\%$. The red dashed line is the $1/n_{e,ped}$, fit to the square markers with a $\chi = 3\%$.

5. Discussion

The results from Figs. 4a and 4b suggest that placing the neutral source at the X-point, and measuring the density profile at the OMP, is the reason why the $1/n_{e,ped}$, scaling is not observed within these presented simulations. The strong variation of the E function over the pedestal widths predicted by JETTO-EIRENE is the reason why the $1/n_{e,ped}$, scaling was not observed in the simulations. Accounting for the E function by remapping the density profile from the OMP to a coordinate along the X-point (black line in Fig. 1a) recovers the $1/n_{e,ped}$, scaling within the presented simulations. This suggests that experimental profiles could be remapped in a similar fashion to check whether the $1/n_{e,ped}$, scaling is observed in experiment, noting that the typical experimental width of a JET density pedestal sits within the range which E varies significantly (1–4 cm) [16]. Typically, the density profile is measured (in experiment) at a different poloidal location (e.g. the OMP) to that where the neutral source predominately crosses the separatrix which usually is the X-point (in diverted machines [12]) with neutrals originating from divertor recycling as shown for a particular JET simulation in Fig. 2. Assuming: (i) fixed diffusive transport across the pedestal region; (ii) fixed temperature profiles; (iii) the dominant neutral source is a point source at the X-point due to recycling neutrals (noting that typical neutral flux from a gas valve arriving at the separatrix is an order of magnitude smaller than the recycling flux); (iv) density is a flux surface quantity and (v) density profile is predominantly set by the ionisation source, then experimentally measured pedestal profiles (e.g. from a gas puff scan experiment) could be remapped to the X-point using the method presented in Section 4.2 and the $1/n_{e,ped}$, scaling checked. If the $1/n_{e,ped}$, scaling is experimentally verified via this remapping method, EUROPED [11] could accept a pedestal pressure profile along the X-point coordinate (e.g. black line in Fig. 1a) rather than the usual OMP coordinate. This then would negate the need to have an E factor in Eq. 7 which EUROPED uses to calculate $n_{e,ped}$, based on a fixed Δ_{ne}, because $x = x_m$. However, the predicted pedestal widths and height would be given at the X-point and not the OMP.

In reality a balance of the source, transport and stability most likely sets the pedestal structure; the relative contribution of each is not yet fully understood. The presented simulations considered cases for fixed temperature profiles, transport profiles and neutral velocity, allowing only the density to vary in response to an ionisation source and CX, from a point source of neutrals located at the separatrix. This work has only addressed some of the assumptions made by the NPM and relaxed them, namely the position of the neutral source (testing whether E can be assumed scalar) and the fixed ionisation rate. Future work would need to continue to relax these assumptions to investigate what impact they would have individually and collectively on the $1/n_{e,ped}$, scaling. In reality, the transport in the pedestal region does vary and is thus likely not well described by a fixed diffusive coefficient and so relaxing this condition is paramount in future work. Furthermore, the poloidal neutral source has been assumed to be a point source however it likely enters over some poloidal angle (Fig. 2). Thus choosing a more realistic poloidal source distribution would also need be tested in future work.

The neutral opacity of the edge of a $Q = 10$ ITER DT plasma is expected to be much larger than current machines, meaning neutrals originating from recycling or gas puffing will penetrate the confined plasma significantly less than on current machines [24,25]. Modelling of the ITER density profile has showed almost no density pedestal because within the simulation the edge source became insignificant when no inward pinch is assumed [26]. If the edge neutral source no longer plays a role in establishing the density pedestal, i.e. little to no ionisation of penetrating neutrals (originating from divertor recycling or gas puff) into the confined plasma, the usefulness of the NPM is diminished for predicting reactor pedestals.

Within this analysis, CX has been discounted as a potential mechanism for affecting the density profile. However, it should be noted that CX in the SOL/divertor and fast reflection at the divertor targets could play a role in setting the density profile in the confined region [23]. This analysis has only examined CX within the confined plasma and as such cannot capture CX or fast reflection from outside the separatrix.

6. Conclusion

Neutral source scans have been conducted in JETTO-EIRENE to compare to the neutral penetration model (NPM) [10] and its predictions. A prediction of the NPM is that the density pedestal top ($n_{e,ped}$,) is inversely proportional to the density pedestal width (Δ_{ne},) which is of interest as a simple density pedestal predictor. It was found that on JET the poloidal flux expansion function E (a variable within the NPM), varies with the radial coordinate x which the density is defined along. The E function relates poloidal position at which the density profile is measured, i.e. the diagnostic line of sight, and the poloidal position of the dominant neutral source. The implication of the radially varying E function is that over the range of pedestal widths explored in the density scan no single E value can characterise the whole data set. Hence $1/n_{e,ped}$, scaling is not valid because it is derived on the assumption that a constant E will describe the whole density scan. Indeed this is what is observed within the simulations. When performing a density scan where the source is placed at the OMP and the measured density profile is at the OMP (i.e. $E = 1$), the $1/n_{e,ped}$, scaling is observed. However, placing the neutral source at the X-point (a more realistic assumption - Fig. 2 and Ref. [12]) and preforming a density scan, measuring the resultant density profile at the OMP, Δ_{ne}, does not scale as $1/n_{e,ped}$, but more as $1/n_{e,ped}^2$. The $1/n_{e,ped}$, scaling was recovered in the simulations with neutral source placed at the X-point, by remapping the density profile from the OMP to the X-point. This results in the measurement coordinate being the same as the coordinate which the neutrals were injected, which accounts properly for the fact that E varies over the range of density pedestal widths explored. The same process of remapping the simulated density profiles could be applied to experimental density profiles (e.g. a gas scan). Remapping the experimental density profile from the line of sight of measurement to the X-point could be performed in order to confirm whether the $1/n_{e,ped}$, scaling is observed experimentally.

The NPM also assumes that the ionisation rate is constant and that there is no charge exchange. Within our density scans, we tested this assumption by allowing a spatially varying ionisation rate and activated charge exchange within the neutral model. Minimal deviation was observed from the $1/n_{e,ped}$, scaling when these assumptions were relaxed suggesting they are indeed reasonable.

Declaration of Competing Interest

The authors declare that they have no known competing financial interests or personal relationships that could have appeared to influence the work reported in this paper.

Acknowledgements

I would like to thank Alex Chankin for providing the EDGE2D-EIRENE simulation of the JET discharge 92168 which was integral in setting the boundary conditions for the JETTO-EIRENE simulations.

This work has been carried out within the framework of the EUROfusion Consortium and has received funding from the Euratom research and training programme 2014–2018 and 2019–2020 under grant agreement No 633053. The views and opinions expressed herein do not necessarily reflect those of the European Commission.

References

[1] F. Wagner et al., Regime of improved confinement and high beta in neutral-beam-heated divertor discharges of the asdex tokamak, Phys. Rev. Lett., vol. 49, pp. 1408–1412, 19 1982. doi: 10.1103/PhysRevLett. 49.1408.

[2] X. Garbet et al., Profile stiffness and global confinement, Plasma Physics and Controlled Fusion, vol. 46, no. 9, pp. 1351–1373, 2004, issn: 07413335. doi: 10.1088/0741-3335/46/9/002.

[3] E.D. (T. Physics) et al., Chapter 2: Plasma confinement and transport, Nuclear Fusion, vol. 47, no. 6, S18–S127, 2007. doi: 10. 1088/ 0029 - 5515/47/6/s02.

[4] P.B. Snyder et al., Development and validation of a predictive model for the pedestal height, Physics of Plasmas, vol. 16, no. 5, 2009, issn: 1070664X. doi: 10.1063/1.3122146.

[5] P.B. Synder, A first-principles predictive model of the pedestal height and width: development, testing and ITER optimization with the EPED model Related content, Nuclear Fusion 51 (10) (Aug. 2011) 103–116, https://doi.org/10.1088/0029-5515/51/10/103016.

[6] C.F. Maggi et al., Studies of the pedestal structure and inter-ELM pedestal evolution in JET with the ITER-like wall, Nuclear Fusion, vol. 57, no. 11, aa7-e8e, 2017, issn: 17414326. doi: 10.1088/1741-4326/aa7e8e.

[7] E.D. Luna et al., Recent Results on High-Triangularity H-mode Studies in JET-ILW, pp. 1-8, 2014.

[8] C. Giroud et al., Progress at JET in integrating ITER-relevant core and edge plasmas within the constraints of an ITER-like wall, Plasma Physics and Controlled Fusion, vol. 57, no. 3, 2015, issn: 13616587. doi: 10.1088/0741-3335/57/3/035004.

[9] J.W. Hughes et al., Edge profile stiffness and insensitivity of the density pedestal to neutral fuelling in Alcator C-Mod edge transport barriers, Nuclear Fusion, vol. 47, no. 8, pp. 1057–1063, Aug. 2007, issn: 00295515. doi: 10. 1088/ 0029 - 5515/ 47/ 8/ 041.

[10] R.J. Groebner et al., The role of neutrals in high-mode (H-mode) pedestal formation, Physics of Plasmas, vol. 9, no. 5, pp. 2134–2140, 2002, issn: 1070664X. doi: 10.1063/1.1462032.

[11] S. Saarelma et al., Integrated modelling of H-mode pedestal and confinement in JET-ILW, Plasma Physics and Controlled Fusion, vol. 60, no. 1 2018, issn: 13616587. doi: 10.1088/1361-6587/aa8d45.

[12] M. Groth et al., Poloidal distribution of recycling sources and core plasma fueling in DIII-D, ASDEX-Upgrade and JET L-mode plasmas, Plasma Physics and Controlled Fusion, vol. 53, no. 12, 2011, issn: 07413335. doi: 10.1088/0741-3335/53/12/124017.

[13] L.W. Owen et al., Origins and spatial distributions of core fueling in the DIII-D tokamak, Journal of Nuclear Materials, vol. 290–293, pp. 464–468, Mar. 2001, issn: 00223115. doi: 10.1016/S0022-3115(00)00582-1.

[14] J.W. Hughes et al., Advances in measurement and modeling of the high confinement-mode pedestal on the Alcator C-Mod tokamak, in Physics of Plasmas, vol. 13, American Institute of PhysicsAIP, May 2006, p. 056 103. doi: 10.1063/1.2180748. [Online]. Available: http://aip.scitation. org/doi/10.1063/1.2180748.

[15] R. Groebner, Progress towards a predictive model for pedestal height in DIII-D Related content Temporal evolution of H-mode pedestal in DIIID-Limits to the H-mode pedestal pressure gradient in DIII-D, 2009. doi: 10.1088/0029-5515/49/8/085037.

[16] M.J. Leyland et al., The H-mode pedestal structure and its role on confinement in JET with a carbon and metal wall, Nuclear Fusion, vol. 55, no. 1, 2015, issn: 17414326. doi: 10.1088/0029-5515/55/1/013019.

[17] R. Scannell et al., Deconvolution of Thomson scattering temperature profiles, Review of Scientific Instruments, vol. 82, no. 5, 2011, issn: 00346748. doi: 10.1063/1.3581230.

[18] C. Giroud et al., IAEA Fusion Energy Conference, Gandhinagar, EX/3-3, 2018.

[19] R. Simonini et al., Models and Numerics in the Multi-Fluid 2-D Edge Plasma Code EDGE2D/U, Contributions to Plasma Physics, vol. 34, no. 2–3, pp. 368–373, Jan. 1994, issn: 08631042. doi: 10.1002/ctpp. 2150340242.

[20] D. Reiter, Progress in two-dimensional plasma edge modelling, J. Nuclear Mater. 471 (1992) 196.

[21] M. Romanelli, et al., Luca GARZOTTI 1), Derek HARTING 1), Florian KÖCHL 1,5), Tuomas KOSKELA 1,6), Elina MILITELLO-ASP 9 (8) (2014), https://doi.org/10.1585/pfr.9.3403023.

[22] D. Reiter, The data file HYDHEL: Atomic and Molecular Data for EIRENE based upon: Janev, Langer, Evans, Post, Elementary Processes in Hydrogen-Helium Plasmas, Springer 1987 FZ, Forschungszentrum J ulich GmbH FRG Available via E-mail from d.reiter@fz-jueli, pp. 12–16, 1987.

[23] A. Kukushkin, et al., Finalizing the iter divertor design: The key role of solps modeling, Fusion Engineering and Design 86 (12) (2011) 2865–2873, https://doi.org/10.1016/j.fusengdes.2011.06.009.

[24] A. Kukushkin, et al., Analysis of performance of the optimized divertor in ITER, Nuclear Fusion 49 (7) (2009), 075–008, 2009. https://doi.org/10.1088/0029-5515/49/7/075008.

[25] M. Romanelli, et al., Modelling of plasma performance and transient density behaviour in the h-mode access for ITER gas fuelled scenarios, Nuclear Fusion 55 (9) (2015), 093–008. https://doi.org/10.1088/0029-5515/55/9/093008.

[26] T. Lunt et al., Influence of the first wall material on the particle fuelling in ASDEX Upgrade, Plasma Physics and Controlled Fusion, vol. 59, no. 5, p. 55 016, 2017, issn: 13616587. doi: 10.1088/1361-6587/aa659f.